
PERGAMON

Journal of the Mechanics and Physics of Solids
50 (2002) 471–500

JOURNAL OF THE
MECHANICS AND
PHYSICS OF SOLIDS

www.elsevier.com/locate/jmps

Green's function for incremental nonlinear elasticity: shear bands and boundary integral formulation

Davide Bigoni[a,*], Domenico Capuani[b]

[a] *Dipartimento di Ingegneria Meccanica e Strutturale, Università di Trento, Via Mesiano 77-38050 Povo, Trento, Italy*

[b] *Dipartimento di Ingegneria, Università di Ferrara, Via Saragat 1-44100 Ferrara, Italy*

Received 6 December 2000; accepted 5 April 2001

Abstract

An elastic, incompressible, infinite body is considered subject to plane and homogeneous deformation. At a certain value of the loading, when the material is still in the elliptic range, an incremental concentrated line load is considered acting at an arbitrary location in the body and extending orthogonally to the plane of deformation. This plane strain problem is solved, so that a Green's function for incremental, nonlinear elastic deformation is obtained. This is used in two different ways: to quantify the decay rate of self-equilibrated loads in a homogeneously stretched elastic solid; and to give a boundary element formulation for incremental deformations superimposed upon a given homogeneous strain. The former result provides a perturbative approach to shear bands, which are shown to develop in the elliptic range, induced by self-equilibrated perturbations. The latter result lays the foundations for a rigorous approach to boundary element techniques in finite strain elasticity.

Keywords: Green's function; Nonlinear elasticity; Shear bands; Boundary element method

1. Introduction

The determination of Green's functions and related integral representations of elastic states are classical problems in the linear theory of elasticity. In this context, different classes of anisotropies have been considered for static and dynamic situations (Love, 1927; Lifshitz and Rozentsveig, 1947; Willis, 1965, 1973; Pan and Chou, 1976; more recently, see Ting and Lee, 1997 and references cited therein).

* Corresponding author. Tel.: +39-0461-8825-07; fax: +39-0461-8825-99.
E-mail addresses: bigoni@ing.unitn.it (D. Bigoni), cpd@dns.unife.it (D. Capuani).

0022-5096/02/$ - see front matter
PII: S0022-5096(01)00090-4

An infinite-body Green's function is obtained in the present article for incremental, nonlinear elastic, isochoric deformation. To this purpose, the simplest setting is chosen, corresponding to the Biot problem in which an infinite medium is homogeneously and biaxially deformed an arbitrary amount within the elliptic range. The current configuration is plane strain and characterized by two in-plane stretches. The incremental response of this incompressible solid is linear and governed by the two Biot (1965) moduli, which are functions of the in-plane stretches.

At a generic stage of this deformation path, an incremental point load is superimposed so that the plane strain constraint is not violated. The corresponding velocity problem is solved and the nominal stress rate distribution is obtained. The singular solution is worked out by using the plane-wave expansion method (John, 1955; Courant and Hilbert, 1962; Gel'fand and Shilov, 1964) in the stream function formulation of Hill and Hutchinson (1975). The result is new, even in the trivial case when the current stress is null, but is in a sense expected, since our problem may be viewed as a special case of the general formulation given by Willis (1991). In fact, singular solutions for concentrated loads on the free boundary of an elastic, pre-stressed half-space have already been obtained (Green et al., 1952; Green and Zerna, 1968; Beatty and Usmani, 1975; Dhaliwal and Singh, 1978; Filippova, 1978; Guz' et al. 1998), but surprisingly—with the remarkable exception of Willis (1991)—the case of an infinite medium was not considered. The solution relative to the infinite medium is however important from different points of view, two of which will be analyzed in detail, namely:

- the evaluation of decay rates of self-equilibrated loads in incremental, nonlinear elasticity;
- the formulation of boundary element for incremental deformations superimposed upon a given homogeneous strain.

The problem of the evaluation of decay rates of self-equilibrated loads in linear elasticity is related to the determination of the extent of local effects and to Saint Venant's principle. The topic has been thoroughly analyzed starting from pioneering works of Zanaboni (1937) and Mises (1945) [see Gurtin (1972) and the review papers by Horgan (1989, 1996)]. In nonlinear elasticity, the situation is much different, and only few contributions are available. Our interest here is in evaluating decay effects when small deformations are superimposed on large deformations. In this context, semi-infinite, pre-stressed strips subjected to self-equilibrated, incremental end loads have been analyzed by Abeyaratne et al. (1985) and Durban and Stronge (1988). A self-equilibrated incremental load acting at an arbitrary stage of homogeneous deformation of a nonlinear elastic continuum is considered in the present paper. Our analysis is based on the availability of the singular solution for the point load; in particular, the effects are investigated of a dipole, i.e. a self-equilibrated loading given by two equal but opposite point loads. The solution is obtained by superposition, since the incremental problem is linear. With the solution of this second problem in hand, we quantify the decay rate of the self-equilibrated load. This is a function of the current in-plane stretches or, in other words, of the current state of stress. When the latter is reduced to zero, a linear elastic solution is obtained, which decays rapidly away from the load. On the other

hand, the solution is shown to blow up when the boundary of the elliptic range is approached. In this limit the decay distance becomes infinite. Interestingly, it is shown that, approaching the elliptic boundary, the incremental solution tends to self-organize along well-defined shear band patterns. This provides a perturbative approach to strain localization, which is shown to be *induced by a perturbation while the deformation is still in the elliptic range*.

Finally, the obtained Green's function is shown to be useful for the solution of boundary value problems where incremental deformations are superimposed upon a given, homogeneous strain. To this purpose, we provide an integral boundary representation for velocity and in-plane hydrostatic stress rate. This, in the very particular case of null current stress and incremental isotropy, formally coincides with the representation given by Ladyzhenskaya (1963) for Navier–Stokes flow. The integral representation, together with the fundamental solution allows us to formulate a boundary element technique for the incremental, homogeneous problem. A relevant advantage of the boundary element approach is in dealing with the incompressibility constraint, which is inherent in our formulation. To provide an example of the capabilities of the proposed approach, we solve the problem of transversal incremental loading of a Mooney–Rivlin elastic block subjected to a compressive axial load. In this case, the bifurcation load, corresponding to a symmetric surface mode, is obtained through a perturbative, numerical approach.

We believe that the fundamental solution and the integral formulation derived here provide a first step towards a rigorous application of the boundary element method to large strain elastic problems.

2. Constitutive equations

Under plane strain conditions, the most general constitutive equations for a hyperelastic, initially isotropic, incompressible solid have been given by Biot (1965) and can conveniently be expressed in the principal reference system of Cauchy stress (here denoted by indices 1 and 2). In this system, using a Lagrangean formulation of the field equations with the current state taken as reference, the relation between material time derivative of nominal stress t_{ij} and velocity gradient $v_{i,j}$ can be written as

$$\dot{t}_{ij} = \mathbb{K}_{ijkl} v_{l,k} + \dot{p}\delta_{ij}, \tag{1}$$

where a comma denotes partial differentiation, repeated indices are summed and range between 1 and 2, δ_{ij} is the Kronecker delta, $\dot{p}$ the in-plane hydrostatic stress rate and $\mathbb{K}_{ijkl}$ are the instantaneous moduli. These possess the major symmetry $\mathbb{K}_{ijkl} = \mathbb{K}_{klij}$ and are functions of the components of Cauchy stress σ_1 and σ_2 and of two incremental moduli μ and μ_*, denoting respectively the moduli corresponding to shearing parallel to, and at 45° to, the principal stress axes. The components of $\mathbb{K}_{ijkl}$ different from zero are

$$\begin{aligned} &\mathbb{K}_{1111} = \mu_* - \frac{\sigma}{2} - p, \quad \mathbb{K}_{1122} = \mathbb{K}_{2211} = -\mu_*, \quad \mathbb{K}_{2222} = \mu_* + \frac{\sigma}{2} - p, \\ &\mathbb{K}_{1212} = \mu + \frac{\sigma}{2}, \quad \mathbb{K}_{1221} = \mathbb{K}_{2112} = \mu - p, \quad \mathbb{K}_{2121} = \mu - \frac{\sigma}{2}, \end{aligned} \tag{2}$$

with

$$\sigma = \sigma_1 - \sigma_2, \quad p = \frac{\sigma_1 + \sigma_2}{2}. \tag{3}$$

In addition to Eq. (1), incompressibility requires that the velocity field v_i be solenoidal:

$$v_{i,i} = 0. \tag{4}$$

The constitutive framework described by the above equations is quite broad and includes, for instance, the relevant cases of Mooney–Rivlin, Ogden materials and J_2-deformation theory material, introduced by Hutchinson and Neale (1979). In the Mooney–Rivlin case, the incremental moduli and the deviatoric stress σ depend on the maximum current stretch $\lambda > 1$,

$$\sigma = \mu_0\,(\lambda^2 - \lambda^{-2}), \quad \mu_* = \mu = \frac{\mu_0}{2}(\lambda^2 + \lambda^{-2}), \tag{5}$$

through the ground-state shear modulus μ_0. Constitutive equations (5) can be written in a more general form, which includes the Ogden material, as (Ogden, 1984)

$$\sigma = \sum_{i=1}^{N} \mu_i(\lambda^{\beta_i} - \lambda^{-\beta_i}), \quad \mu_* = \frac{1}{4}\sum_{i=1}^{N} \mu_i\beta_i(\lambda^{\beta_i} + \lambda^{-\beta_i}),$$

$$\mu = \frac{1}{2}\frac{\lambda^4 + 1}{\lambda^4 - 1}\sum_{i=1}^{N} \mu_i(\lambda^{\beta_i} - \lambda^{-\beta_i}), \tag{6}$$

where μ_i and β_i are material parameters.

It may be important to note that constitutive equations (1) and (2) describe also the incremental behavior of materials which are *initially orthotropic* with respect to directions 1 and 2. In the interest of generality, no specific assumptions will be introduced on the dependence of μ_* and μ on the current state.

3. The Green's function set

At an arbitrary stage of a homogeneous, plane deformation of an infinite medium, we consider an incremental force (a line loading extending orthogonally to the plane of deformation) acting at the point $\boldsymbol{x} = \boldsymbol{0}$ and with components $\dot{f}_1, \dot{f}_2$ along the principal stress axes. The incremental equilibrium equations are

$$\dot{t}_{ij,i} + \dot{f}_j\delta(\boldsymbol{x}) = 0, \tag{7}$$

where δ is the two-dimensional Dirac delta function and $\boldsymbol{x}$ denotes the generic material point. Employing the constitutive equations and assuming a homogeneous current state, Eqs. (7) become, in explicito

$$(2\mu_* - p)v_{1,11} + (\mu - p)v_{2,12} + \left(\mu - \frac{\sigma}{2}\right)v_{1,22} + \dot{f}_1\delta(\boldsymbol{x}) = -\dot{\pi}_{,1},$$

$$(2\mu_* - p)v_{2,22} + (\mu - p)v_{1,21} + \left(\mu + \frac{\sigma}{2}\right)v_{2,11} + \dot{f}_2\delta(\boldsymbol{x}) = -\dot{\pi}_{,2}, \tag{8}$$

where

$$\dot{\pi} = \frac{\dot{t}_{11} + \dot{t}_{22}}{2} = \dot{p} - \frac{\sigma}{2} v_{1,1}. \tag{9}$$

It is expedient to introduce a stream function $\psi(x_1, x_2)$ defining a solenoidal but otherwise arbitrary velocity field

$$v_1 = \psi_{,2}, \quad v_2 = -\psi_{,1}, \tag{10}$$

so that by differentiating Eqs. $(8)_1$ and $(8)_2$ with respect to x_2 and x_1, respectively, and subtracting the results, we obtain

$$\left(\mu + \frac{\sigma}{2}\right) \psi_{,1111} + 2(2\mu_* - \mu)\psi_{,1122} + \left(\mu - \frac{\sigma}{2}\right) \psi_{,2222} + \dot{f}_1 \delta_{,2} - \dot{f}_2 \delta_{,1} = 0. \tag{11}$$

It is worth noting that when $\sigma = 0$ and $\mu_* = \mu$, Eq. (11) becomes formally identical to the stream function equation of Navier–Stokes model for incompressible, plane, viscous flow (Ladyzhenskaya, 1963, Section 2.3).

The standard regime classification is performed on the basis of the characteristic equation associated to Eq. (11). To this purpose, we define

$$k = \frac{\sigma}{2\mu}, \tag{12}$$

which, without loss of generality, may always be taken to be nonnegative (simply orienting axes 1 and 2 in a proper way). The equation defining the regime classification can therefore be written as

$$\mu\omega_2^4 \left[(1+k)\frac{\omega_1^4}{\omega_2^4} + 2\left(2\frac{\mu_*}{\mu} - 1\right)\frac{\omega_1^2}{\omega_2^2} + (1-k)\right] = 0. \tag{13}$$

Eq. (13) admits

- no real solution ω_1/ω_2 in the elliptic regime (E);
- four real solutions ω_1/ω_2 in the hyperbolic regime (H);
- two real solutions ω_1/ω_2 in the parabolic regime (P).

The elliptic regime, where $k < 1$, may be further sub-divided into elliptic complex (EC) and elliptic imaginary (EI) regimes. In particular, Eq. (13) admits

- two conjugate pairs of complex solutions ω_i in the elliptic complex regime (EC);
- four purely imaginary solutions (in conjugate pairs) ω_i in the elliptic imaginary regime (EI).

If we explicitly introduce the roots for ω_1^2/ω_2^2 of Eq. (13)

$$(1+k)\frac{\omega_1^4}{\omega_2^4} + 2\left(2\frac{\mu_*}{\mu} - 1\right)\frac{\omega_1^2}{\omega_2^2} + 1 - k = (1+k)\left[\frac{\omega_1^2}{\omega_2^2} - \gamma_1\right]\left[\frac{\omega_1^2}{\omega_2^2} - \gamma_2\right], \tag{14}$$

where

$$\left.\begin{matrix}\gamma_1 \\ \gamma_2\end{matrix}\right\} = \frac{1 - 2\mu_*/\mu \pm \sqrt{\Delta}}{1+k}, \quad \Delta = k^2 - 4\frac{\mu_*}{\mu} + 4\left(\frac{\mu_*}{\mu}\right)^2, \tag{15}$$

we conclude that γ_1 and γ_2 are both real and negative in the (EI) regime and are a conjugate pair in the (EC) regime. Therefore, Δ is positive in (EI) and negative in (EC).

Note that the Mooney–Rivlin material corresponds to $\Delta = k$ and $\gamma_1 = (k-1)/(k+1)$, $\gamma_2 = -1$.

There are two ways to exit the (E) regime, namely

- crossing the (EI)/(P) boundary. This corresponds to $k = 1$, i.e. γ_1 must vanish;
- crossing the (EC)/(H) boundary. This corresponds to $\Delta = 0$, i.e. the two γ_i's must coincide.

It is worth noting that, when the (EC)/(H) boundary is approached from (E), $\Delta < 0$ and $\mu > 2\mu_*$, whereas $\Delta > 0$ and $\mu < 2\mu_*$, when the (EI)/(P) boundary is approached.

We recall from Biot (1965) and Hill and Hutchinson (1975) that incompressible, elastic materials deformed in plane strain, which are *isotropic in the initial state*, cannot penetrate the (P) regime, so that the (EI)/(P) boundary can be reached only at the limit of infinite stretch.

It is important to note that in the following *we will always assume to remain within the elliptic regime*.

3.1. Determination of the velocity field

We follow here the general procedure proposed by Willis (1971, 1972, 1973) to solve singular problems in the infinitesimal theory of elasticity. Since the incremental problem is linear, the solution pertaining to a generic point load can be obtained as the superposition of the solutions for two forces, one acting along axis 1 and the other along axis 2. With this reference, we may take $\dot{f}_i = \delta_{ig}$ and rewrite Eq. (11) as

$$\mathscr{L}\psi^g + \left(\delta_{1g}\frac{\partial \cdot}{\partial x_2} - \delta_{2g}\frac{\partial \cdot}{\partial x_1}\right)\delta(\boldsymbol{x}) = 0, \tag{16}$$

where $\mathscr{L}$ is the linear differential operator, with constant coefficients, defined as

$$\mathscr{L}(\cdot) = \left(\mu + \frac{\sigma}{2}\right)\frac{\partial^4 \cdot}{\partial x_1^4} + 2(2\mu_* - \mu)\frac{\partial^4 \cdot}{\partial x_1^2 \partial x_2^2} + \left(\mu - \frac{\sigma}{2}\right)\frac{\partial^4 \cdot}{\partial x_2^4}. \tag{17}$$

The plane wave expansion of the δ function is (Courant and Hilbert, 1962; Gel'fand and Shilov, 1964)

$$\delta(\boldsymbol{x}) = -\frac{1}{4\pi^2}\oint_{|\boldsymbol{\omega}=1|}\frac{\mathrm{d}\omega}{(\boldsymbol{\omega}\cdot\boldsymbol{x})^2}, \tag{18}$$

where $\boldsymbol{\omega}$ is the unit vector (Fig. 1), so that defining the analogous transform $\tilde{\psi}^g(\boldsymbol{\omega}\cdot\boldsymbol{x})$ of $\psi^g(\boldsymbol{x})$ as

$$\psi^g(\boldsymbol{x}) = -\frac{1}{4\pi^2}\oint_{|\boldsymbol{\omega}=1|}\tilde{\psi}^g(\boldsymbol{\omega}\cdot\boldsymbol{x})\,\mathrm{d}\omega, \tag{19}$$

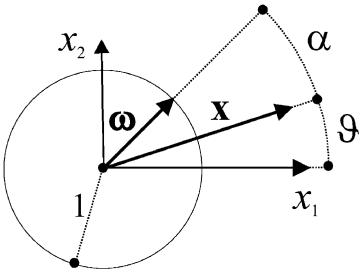

Fig. 1. Reference system, vectors $\boldsymbol{\omega}, \boldsymbol{x}$, and angles ϑ and α.

the transform of Eq. (16) yields

$$\mathscr{L}\tilde{\psi}^g(\boldsymbol{\omega}\cdot\boldsymbol{x}) = 2\frac{\delta_{1g}\omega_2 - \delta_{2g}\omega_1}{(\boldsymbol{\omega}\cdot\boldsymbol{x})^3}. \tag{20}$$

Employing the chain rule of differentiation

$$[\tilde{\psi}^g(\boldsymbol{\omega}\cdot\boldsymbol{x})]_{,k} = \omega_k(\tilde{\psi}^g)', \tag{21}$$

where a prime denotes differentiation with respect to the scalar $\boldsymbol{\omega}\cdot\boldsymbol{x}$, and introducing the function

$$L(\boldsymbol{\omega}) = \mu\omega_2^4(1+k)\left[\frac{\omega_1^2}{\omega_2^2} - \gamma_1\right]\left[\frac{\omega_1^2}{\omega_2^2} - \gamma_2\right] > 0, \tag{22}$$

which is always strictly positive in (E), Eq. (20) becomes

$$L(\boldsymbol{\omega})(\tilde{\psi}^g)'''' = 2\frac{\delta_{1g}\omega_2 - \delta_{2g}\omega_1}{(\boldsymbol{\omega}\cdot\boldsymbol{x})^3}. \tag{23}$$

Integration of differential equation (23) with respect to the variable $\boldsymbol{\omega}\cdot\boldsymbol{x}$ gives

$$\tilde{\psi}^g = \frac{\delta_{1g}\omega_2 - \delta_{2g}\omega_1}{L(\boldsymbol{\omega})}(\boldsymbol{\omega}\cdot\boldsymbol{x})(\log|\boldsymbol{\omega}\cdot\hat{\boldsymbol{x}}| - 1), \tag{24}$$

a formula where additional cubic, quadratic and linear terms in $\boldsymbol{\omega}\cdot\boldsymbol{x}$, representing inessential contributions, have been disregarded. In Eq. (24), $\hat{\boldsymbol{x}}$ represents a dimensionless measure of distance, i.e. $\boldsymbol{x}$ is divided by any characteristic length. The antitransform of Eq. (24) determines the stream function

$$\psi^g = -\frac{1}{4\pi^2}\oint_{|\boldsymbol{\omega}=1|}\frac{\delta_{1g}\omega_2 - \delta_{2g}\omega_1}{L(\boldsymbol{\omega})}(\boldsymbol{\omega}\cdot\boldsymbol{x})(\log|\boldsymbol{\omega}\cdot\hat{\boldsymbol{x}}| - 1)\,\mathrm{d}\omega, \tag{25}$$

which may be expanded to yield

$$\begin{aligned}\psi^g = -\frac{r}{2\pi^2\mu(1+k)}\Bigg[&(\log\hat{r} - 1)\int_0^{\pi}\frac{\sin[\alpha+\vartheta+(1-g)\pi/2]\cos\alpha}{\Lambda(\alpha+\vartheta)}\,\mathrm{d}\alpha \\ &+\int_0^{\pi/2}\frac{\sin[\alpha+\vartheta+(1-g)\pi/2]\cos\alpha\log(\cos\alpha)}{\Lambda(\alpha+\vartheta)}\,\mathrm{d}\alpha \\ &-\int_0^{\pi/2}\frac{\cos[\alpha+\vartheta-(g-1)\pi/2]\sin\alpha\log(\sin\alpha)}{\Lambda(\alpha+\vartheta+\pi/2)}\,\mathrm{d}\alpha\Bigg],\end{aligned} \tag{26}$$

where, with reference to Fig. 1, the distance $r=|\boldsymbol{x}|$ and the angle ϑ are polar coordinates, $\hat{r}$ is a dimensionless measure of distance, and

$$\Lambda(\alpha)=\sin^4\alpha[\cot^2\alpha-\gamma_1][\cot^2\alpha-\gamma_2]>0. \tag{27}$$

The Green's tensor for the infinite body represents the velocity field associated with stream function (26) and, according to Eq. (10), is given by

$$v_1^g=\frac{\partial\psi^g}{\partial x_2},\quad v_2^g=-\frac{\partial\psi^g}{\partial x_1}. \tag{28}$$

The tensor components (28) have to satisfy the identity

$$v_1^2=v_2^1, \tag{29}$$

which may be directly verified using Eq. (28) in Eq. (26) and, more in general, is a consequence of the major symmetry of $\mathbb{K}_{ijkl}$. Employing Eqs. (25) and (28), we obtain

$$v_i^g=-\frac{1}{4\pi^2}\oint\limits_{|\boldsymbol{\omega}=1|}\tilde{v}_i^g(\boldsymbol{\omega}\cdot\boldsymbol{x})\,\mathrm{d}\omega, \tag{30}$$

where

$$\tilde{v}_i^g(\boldsymbol{\omega}\cdot\boldsymbol{x})=(\delta_{1i}\omega_2-\delta_{2i}\omega_1)(\delta_{1g}\omega_2-\delta_{2g}\omega_1)\frac{\log|\boldsymbol{\omega}\cdot\hat{\boldsymbol{x}}|}{L(\boldsymbol{\omega})}. \tag{31}$$

With the coordinate system of Fig. 1, the components of the Green's tensor (30) take the expression

$$\begin{aligned}v_m^g=\frac{1}{2\pi^2\mu(1+k)}\Bigg[&\log\hat{r}\int_0^\pi\frac{\sin[\alpha+(1-m)\pi/2]\cos[\alpha+(2-g)\pi/2]}{\Lambda(\alpha)}\,\mathrm{d}\alpha\\&+\int_0^\pi\frac{\sin[\alpha+\vartheta+(1-m)\pi/2]\cos[\alpha+\vartheta+(2-g)\pi/2]\log|\cos\alpha|}{\Lambda(\alpha+\vartheta)}\,\mathrm{d}\alpha\Bigg],\end{aligned} \tag{32}$$

where the integrals independent of ϑ can be evaluated, yielding

$$\begin{aligned}v_1^1=&\frac{\log\hat{r}}{2\pi\mu(1+k)}\frac{1}{\gamma_1\sqrt{-\gamma_2}+\sqrt{-\gamma_1}\,\gamma_2}\\&-\frac{1}{2\pi^2\mu(1+k)}\int_0^{\pi/2}\frac{\log(\cos\alpha)\sin^2(\alpha+\vartheta)}{\Lambda(\alpha+\vartheta)}\,\mathrm{d}\alpha\\&-\frac{1}{2\pi^2\mu(1+k)}\int_0^{\pi/2}\frac{\log(\sin\alpha)\cos^2(\alpha+\vartheta)}{\Lambda(\alpha+\vartheta+\pi/2)}\,\mathrm{d}\alpha,\\v_2^2=&-\frac{\log\hat{r}}{2\pi\mu(1+k)}\frac{1}{\sqrt{-\gamma_1}+\sqrt{-\gamma_2}}-\frac{1}{2\pi^2\mu(1+k)}\int_0^{\pi/2}\frac{\log(\cos\alpha)\cos^2(\alpha+\vartheta)}{\Lambda(\alpha+\vartheta)}\,\mathrm{d}\alpha\\&-\frac{1}{2\pi^2\mu(1+k)}\int_0^{\pi/2}\frac{\log(\sin\alpha)\sin^2(\alpha+\vartheta)}{\Lambda(\alpha+\vartheta+\pi/2)}\,\mathrm{d}\alpha,\end{aligned}$$

$$v_2^1 = v_1^2 = \frac{1}{2\pi^2\mu(1+k)}\int_0^{\pi/2}\cos(\alpha+\vartheta)\sin(\alpha+\vartheta) \times\left(\frac{\log(\cos\alpha)}{\Lambda(\alpha+\vartheta)} - \frac{\log(\sin\alpha)}{\Lambda(\alpha+\vartheta+\pi/2)}\right)\mathrm{d}\alpha. \tag{33}$$

In Eq. (33), the dependence on r is explicit and the integrals are improper Riemann integrals which may easily be shown to converge. Therefore, the numerical treatment of Eq. (33) is straightforward, at least for material parameters not too close to the (E) boundary (see Section 4). Moreover, it is easy to show that the components of the Green's function (33) satisfy the following symmetries:

$$v_i^i(\vartheta) = v_i^i(-\vartheta) = v_i^i(\pi-\vartheta), \quad v_2^1(\vartheta) = -v_2^1(-\vartheta) = -v_2^1(\pi-\vartheta),$$
$$v_2^1(0) = v_2^1(\pi/2) = 0 \tag{34}$$

(with $i=1,2$) so that ϑ can be restricted to range within $[0,\pi/2]$.

In the limit case of infinitesimal theory ($k=0$) and isotropic elasticity ($\mu=\mu_*$, $\gamma_1=\gamma_2=-1$), Eq. (33) returns the well-known Green's function for Stokes flow (Ladyzhenskaya, 1963, Section 3.4):

$$v_m^m = -\frac{\log\hat{r}}{4\pi\mu} + \frac{3-2m}{8\pi\mu}\cos(2\vartheta), \quad v_2^1 = \frac{1}{4\pi\mu}\sin\vartheta\cos\vartheta. \tag{35}$$

3.2. Determination of the velocity gradient

The velocity gradient associated to the Green's tensor is given by

$$\frac{\partial v_i^g}{\partial x_1} = \cos\vartheta\frac{\partial v_i^g}{\partial r} - \frac{\sin\vartheta}{r}\frac{\partial v_i^g}{\partial\vartheta}, \quad \frac{\partial v_i^g}{\partial x_2} = \sin\vartheta\frac{\partial v_i^g}{\partial r} + \frac{\cos\vartheta}{r}\frac{\partial v_i^g}{\partial\vartheta}. \tag{36}$$

It should be noted that due to symmetry of Green's tensor (29) and the incompressibility constraint (4), we have

$$v_{2,2}^1 = v_{1,2}^2 = -v_{1,1}^1, \quad v_{2,1}^1 = v_{1,1}^2 = -v_{2,2}^2,$$

so that only four components of the velocity gradient are to be determined. Moreover, Eqs. (33) have a form in which the dependence on r is explicit and the dependence on ϑ involves an integral. Therefore, the derivatives with respect to r yield a singularity of the order $1/r$, whereas the derivatives with respect to ϑ do not alter the singularity. Hence, the velocity gradient can be expressed as

$$v_{1,g}^1 = \frac{1}{2\pi^2\mu(1+k)r}\left[\frac{\pi\cos[\vartheta+(1-g)\pi/2]}{\gamma_1\sqrt{-\gamma_2}+\sqrt{-\gamma_1}\gamma_2} + \sin[\vartheta+(1-g)\pi/2] \times\int_0^{\pi/2}(\log(\cos\alpha)\Sigma(\alpha+\vartheta,\alpha+\vartheta) + \log(\sin\alpha)\Sigma(\alpha+\vartheta+\pi/2,\alpha+\vartheta+\pi/2))\,\mathrm{d}\alpha\right],$$

$$v_{2,g}^2 = -\frac{1}{2\pi^2\mu(1+k)r}\left[\frac{\pi\cos[\vartheta+(1-g)\pi/2]}{\sqrt{-\gamma_1}+\sqrt{-\gamma_2}} - \sin[\vartheta+(1-g)\pi/2]\right.$$
$$\times\int_0^{\pi/2}(\log(\cos\alpha)\Sigma(\alpha+\vartheta+\pi/2,\alpha+\vartheta)$$
$$\left.+\log(\sin\alpha)\Sigma(\alpha+\vartheta,\alpha+\vartheta+\pi/2))\,\mathrm{d}\alpha\right], \tag{37}$$

where

$$\Sigma(\gamma,\eta)=\frac{\sin(\gamma)[2\cos(\gamma)\Lambda(\eta)-\Lambda'(\eta)\sin(\gamma)]}{\Lambda^2(\eta)},\quad \Lambda'(\eta)=\frac{\partial\Lambda(\eta)}{\partial\eta}. \tag{38}$$

3.3. Determination of the incremental stress field

Once the velocity gradient is known, the part of nominal stress rate linearly related to it can be obtained from Eq. (1), but the in-plane hydrostatic stress rate $\dot{p}$ (or, equivalently, $\dot{\pi}$) remains unknown. In order to determine $\dot{\pi}$, Eqs. $(8)_1$ and $(8)_2$ can be differentiated with respect to x_1 and x_2, respectively, and summed to get

$$\dot{\pi}_{,11}+\dot{\pi}_{,22}=-2(\mu_*-\mu)(v_{1,111}+v_{2,222})+\frac{\sigma}{2}(v_{1,111}-v_{2,222})-\dot{f}_1\delta_{,1}-\dot{f}_2\delta_{,2}. \tag{39}$$

A substitution of Eq. (30) for the Green velocity field into Eq. (39) with $\dot{f}_i=\delta_{ig}$ provides the following relation in the transformed domain:

$$(\tilde{\pi}^g)''=-2(\mu_*-\mu)[\omega_1^3(\tilde{v}_1^g)'''+\omega_2^3(\tilde{v}_2^g)''']+\frac{\sigma}{2}[\omega_1^3(\tilde{v}_1^g)'''-\omega_2^3(\tilde{v}_2^g)''']$$
$$+2\frac{\omega_1\delta_{1g}+\omega_2\delta_{2g}}{(\boldsymbol{\omega}\cdot\boldsymbol{x})^3}, \tag{40}$$

and, consistently with Eq. (30), the Green hydrostatic nominal stress rate is given by

$$\dot{\pi}^g=-\frac{1}{4\pi^2}\oint_{|\boldsymbol{\omega}=1|}\tilde{\pi}^g(\boldsymbol{\omega}\cdot\boldsymbol{x})\,\mathrm{d}\omega. \tag{41}$$

Integrating Eq. (40) and neglecting inessential contributions lead to

$$\tilde{\pi}^g=-2(\mu_*-\mu)[\omega_1^3(\tilde{v}_1^g)'+\omega_2^3(\tilde{v}_2^g)']+\frac{\sigma}{2}[\omega_1^3(\tilde{v}_1^g)'-\omega_2^3(\tilde{v}_2^g)']+\frac{\omega_1\delta_{1g}+\omega_2\delta_{2g}}{\boldsymbol{\omega}\cdot\boldsymbol{x}}, \tag{42}$$

where according to Eq. (31)

$$(\tilde{v}_i^g)'=\frac{|\boldsymbol{\omega}|^2\delta_{ig}-\omega_i\omega_g}{L(\boldsymbol{\omega})}\frac{1}{\boldsymbol{\omega}\cdot\boldsymbol{x}}, \tag{43}$$

so that we arrive at

$$\tilde{\pi}^g=\frac{\omega_g}{\boldsymbol{\omega}\cdot\boldsymbol{x}}+(2g-3)\frac{\omega_g(1-\omega_g^2)}{(\boldsymbol{\omega}\cdot\boldsymbol{x})L(\boldsymbol{\omega})}\left[2(\mu_*-\mu)(\omega_1^2-\omega_2^2)-\frac{\sigma}{2}\right]. \tag{44}$$

We note that for infinitesimal ($k=0$), isotropic ($\mu_*=\mu$) elasticity, the antitransform of Eq. (44) yields two Cauchy principal value integrals which may be solved to give

$$\dot{\pi}^1=-\frac{\cos\vartheta}{2\pi r},\quad \dot{\pi}^2=-\frac{\sin\vartheta}{2\pi r}. \tag{45}$$

More generally, the antitransform of Eq. (44) is

$$\begin{aligned}\dot{\pi}^1&=-\frac{\cos\vartheta}{2\pi r}+\frac{1}{2\pi^2 r(1+k)}\,\mathrm{P.V.}\int_0^\pi \frac{\sin^2(\alpha+\vartheta)\cos(\alpha+\vartheta)}{\Lambda(\alpha+\vartheta)\cos\alpha}\Gamma(\alpha+\vartheta)\,\mathrm{d}\alpha,\\ \dot{\pi}^2&=-\frac{\sin\vartheta}{2\pi r}-\frac{1}{2\pi^2 r(1+k)}\,\mathrm{P.V.}\int_0^\pi \frac{\sin(\alpha+\vartheta)\cos^2(\alpha+\vartheta)}{\Lambda(\alpha+\vartheta)\cos\alpha}\Gamma(\alpha+\vartheta)\,\mathrm{d}\alpha,\end{aligned} \tag{46}$$

where

$$\Gamma(\alpha)=2\left(\frac{\mu_*}{\mu}-1\right)(2\cos^2\alpha-1)-k. \tag{47}$$

Eqs. (46) contain two Cauchy principal value integrals, singular at $\alpha=\pi/2$; however, due to the fact that the Cauchy principal value of $\int_0^\pi \mathrm{d}\alpha/\cos\alpha$ is zero, the integrals in Eqs. (46) can be evaluated as

$$\begin{aligned}\dot{\pi}^1&=-\frac{\cos\vartheta}{2\pi r}+\frac{1}{2\pi^2 r(1+k)}\int_0^\pi \frac{1}{\cos\alpha}\left(\frac{\sin^2(\alpha+\vartheta)\cos(\alpha+\vartheta)\Gamma(\alpha+\vartheta)}{\Lambda(\alpha+\vartheta)}\right.\\ &\quad\left.+\frac{\cos^2\vartheta\sin\vartheta\Gamma(\vartheta+\pi/2)}{\Lambda(\vartheta+\pi/2)}\right)\mathrm{d}\alpha,\\ \dot{\pi}^2&=-\frac{\sin\vartheta}{2\pi r}-\frac{1}{2\pi^2 r(1+k)}\int_0^\pi \frac{1}{\cos\alpha}\left(\frac{\sin(\alpha+\vartheta)\cos^2(\alpha+\vartheta)\Gamma(\alpha+\vartheta)}{\Lambda(\alpha+\vartheta)}\right.\\ &\quad\left.-\frac{\cos\vartheta\sin^2\vartheta\Gamma(\vartheta+\pi/2)}{\Lambda(\vartheta+\pi/2)}\right)\mathrm{d}\alpha.\end{aligned} \tag{48}$$

The numerical treatment of Eqs. (48) does not present difficulties, at least for material parameters sufficiently distant from the (E) boundary (see Section 4).

The hydrostatic nominal stress rate (48), together with the velocity field (33), represents the Green's function set $\{v_i^g,\dot{\pi}^g\}$ for the homogeneously stretched, infinite elastic body.

4. Decay effects and shear bands

The singular solution previously obtained can be used to analyze the effects of a perturbation superimposed upon a given homogeneous deformation of an infinite, nonlinear elastic body. Since the incremental problem is linear, several self-equilibrated loading systems can be constructed simply superimposing the unit force solution. Here, a dipole—the simplest self-equilibrated perturbation—is considered, corresponding to two equal and opposite incremental forces.

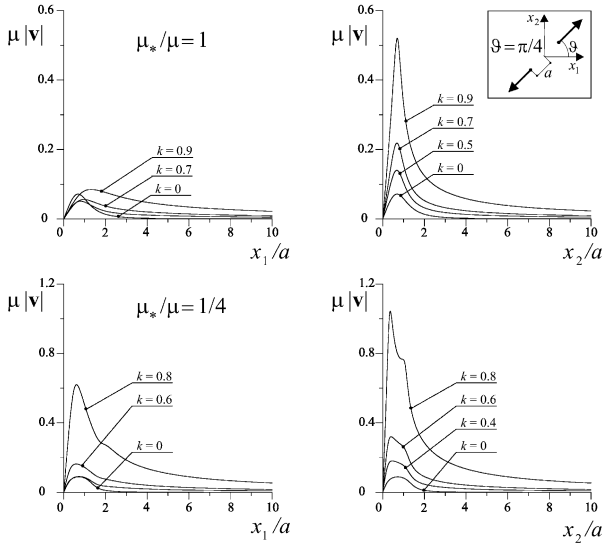

Fig. 2. Decay of the modulus of velocity (multiplicated by μ) along reference axes (x_1/a and x_2/a) for a dipole inclined at 45°.

4.1. Decay properties of self-equilibrated loads

The analysis of the decay effects for self-equilibrated loads is an easy task in our present position. In particular, we consider two equal and opposite unit incremental forces acting at a distance $2a$ and inclined at β with respect to axis x_1. The modulus of velocity $|\boldsymbol{v}|$ for this loading system may be easily evaluated by superposition, using Eqs. (33). For instance, the decay of $|\boldsymbol{v}|$ (multiplied by μ) along axes x_1 and x_2 is reported in Fig. 2 as a function of the dimensionless distances x_1/a and x_2/a for $\mu_*/\mu = 1$ (Mooney–Rivlin material) and for $\mu_*/\mu = 1/4$. In the same figure, the angle $\beta = \pi/4$ has been considered and different values of the pre-stress k are investigated. We may observe from the figure that all the curves initiate at the origin where velocity vanishes, due to symmetry conditions. Moreover, all curves have a similar trend, exhibiting a maximum where the distance to the point of application of the force is minimum, and a subsequent decay to zero. An important feature is the fact that the solution blows up when approaching the (EI)/(P) boundary ($\mu_*/\mu = 1$ and $k = 1$) or the (EC)/(H) boundary ($\mu_*/\mu = 1/4$ and $k \approx 0.866$). Therefore, two important questions arise, namely, whether the modulus of velocity goes to *infinity* when the elliptic boundary is approached, so that decay does not occur, and *how* the solution behaves when the elliptic boundary is approached. We will show below that the answer to the first question is positive and that, concerning the second question, the solution self-organizes along well-defined shear band patterns, geometrically akin to the discontinuous strain rate, occurring only *at* the elliptic boundary.

We start now by considering the velocity field (33) and analyzing the coefficients of the logarithmic terms, when the elliptic boundary is approached.

We note that

- when the (EI)/(P) boundary is approached, $k \to 1$, $\gamma_1 \to 1 - 2\mu_*/\mu\,(<0)$ and $\gamma_2 \to 0^-$, therefore,

$$\frac{1}{\gamma_1\sqrt{-\gamma_2}+\sqrt{-\gamma_1}\gamma_2} \to -\infty \quad \text{and} \quad \frac{1}{\sqrt{-\gamma_1}+\sqrt{-\gamma_2}} \to \frac{1}{\sqrt{2\mu_*/\mu-1}}; \tag{49}$$

- when the (EC)/(H) boundary is approached, $\Delta < 0$,

$$\gamma_1 \to \lim_{\Delta\to 0^-}(1-2\mu_*/\mu+\sqrt{\Delta})/(1+k)$$

$$\text{and} \quad \gamma_2 \to \lim_{\Delta\to 0^-}(1-2\mu_*/\mu-\sqrt{\Delta})/(1+k),$$

therefore,

$$\frac{1}{\gamma_1\sqrt{-\gamma_2}+\sqrt{-\gamma_1}\gamma_2} \to -\infty \quad \text{and} \quad \frac{1}{\sqrt{-\gamma_1}+\sqrt{-\gamma_2}} \to +\infty. \tag{50}$$

In addition to the above terms, we note that the components (33) of the Green's tensor also contain integral terms. Considering now v_2^2 , it is easy to show that the integrands in Eq. $(33)_2$ do not become singular at the (EI)/(P) boundary. Consequently, v_2^2 remains finite when the (EI)/(P) boundary is reached. An analogous property holds true for v_2^1, which remains finite at (EI)/(P). On the contrary, v_1^1 diverges at the (EI)/(P) boundary. Finally, all components of the Green's tensor tend to infinity at the (EC)/(H) limit. These properties are proved in Appendix A.

Let us consider now the dipole. For fixed values of pre-stress and incremental moduli, the solution always decays at infinity. However, as a consequence of the above discussion, the modulus of velocity at fixed points tends to infinity when the elliptic boundary is approached, so that decay does not occur at that limit. On the other hand, the behavior of the velocity components is essentially modified whether the (EI)/(P) or the (EC)/(H) boundary is approached. In particular, all velocity components diverge when approaching the (EC)/(H) boundary, whereas only v_1^1 diverges when approaching the (EI)/(P) boundary. This conclusion preludes the problem analyzed below, namely, how the velocity patterns are modified when the elliptic boundary is approached.

4.2. A perturbative approach to shear bands

As is well known, the formation of shear bands can be viewed as the emergence of discontinuous strain rate patterns. Following Biot (1965) and Hill and Hutchinson (1975), in a continuous, quasi-static path starting from a situation of ellipticity, shear band formation is excluded until the elliptic boundary is reached. In particular, two situations are possible:

- at the (EI)/(P) boundary ($k = 1$) one shear band becomes possible, always aligned parallel to axis 1. For instance, the band is aligned parallel to the tensile axis for uniaxial traction, whereas the band is orthogonal to the compressive direction for uniaxial compression.

- at the (EC)/(H) boundary ($\Delta = 0$) two shear bands become simultaneously possible, equally inclined with respect to the coordinate axes. The inclination η of the normal to the band with respect to axis 1 may be calculated from the following formula:

$$\tan^2 \eta = [1 + 2\sqrt{\mu_*/\mu(1 - \mu_*/\mu)}]/(1 - 2\mu_*/\mu).$$

The above two situations agree with the observation that when the (EI)/(P) boundary is approached from the ellliptic regime, v_2^2 and v_2^1 remain both finite whereas, in contrast, all components v_i^g diverge when the (EC)/(H) boundary is approached. This observation suggests the conjecture that when the elliptic boundary is approached from the interior of the elliptic region, a perturbation in terms of a dipole gives rise to deformation patterns similar to the discontinuous shear bands. Since discontinuous shear bands are only possible *at* the elliptic boundary, our approach provides a perturbative technique to localized deformations. This is confirmed by the qualitative analysis reported in the following.

We consider a self-equilibrated two-force system, centered at the origin of axes, with a distance, say, $2a$ between the two application points of forces. For this perturbation, the streamlines (i.e. the lines $\psi = \text{const.}$) and the level sets of the modulus of velocity (33) are plotted, in a region where the nondimensional coordinate axes x_1/a and x_2/a vary between -5 and 5. Results are reported in Figs. 3–7, for different values of the nondimensional pre-stress k and anisotropy ratio μ_*/μ. Figs. 3–5 pertain to the Mooney–Rivlin case $\mu_*/\mu = 1$ whereas Figs. 6 and 7 to $\mu_*/\mu = 1/4$. Reaching $k = 1$ in the former case corresponds to a point on the (EI)/(P) boundary, whereas reaching $k \approx 0.866$ in the latter case corresponds to a point on the (EC)/(H) boundary. Figs. 3 and 4 are relative to the two forces aligned parallel to axes x_1 and x_2, respectively. In both figures an horizontal shear band appears when k increases. In greater detail, we note the following features:

- the streamlines become parallel along the shear bands, evidencing the shear mode within the band;
- consequent to the initial isotropy, the plots in Fig. 3 can be obtained by a 90° rotation of the plots in Fig. 4 when $k = 0$;
- a shear band progressively emerges in Fig. 3 when k is increased. Vice versa, a shear band is induced by a kind of "Poisson effect" in Fig. 4, where the pre-stress has now a stiffening effect.

The situations analyzed in Figs. 3 and 4 are however peculiar, because the perturbing forces are aligned parallel in one case and orthogonal in the other, to the shear band expected at the elliptic boundary. It is therefore interesting to investigate a generically inclined force system. To this purpose, Fig. 5 is relative to $\beta = \pi/4$ and $k = 0.98$. We note the formation of a mechanism consisting in two horizontal shear bands. Inclinations different from 0 and $\pi/2$ always produce a mechanism with two shear bands. These two shear bands degenerate into a single band at $\beta = 0$ and $\pi/2$. However, the band corresponding to $\beta = 0$ is narrow, compared to the thickness relative to $\beta = \pi/2$. The thickness of the band is related to the parameter a, which introduces a characteristic length in the problem.

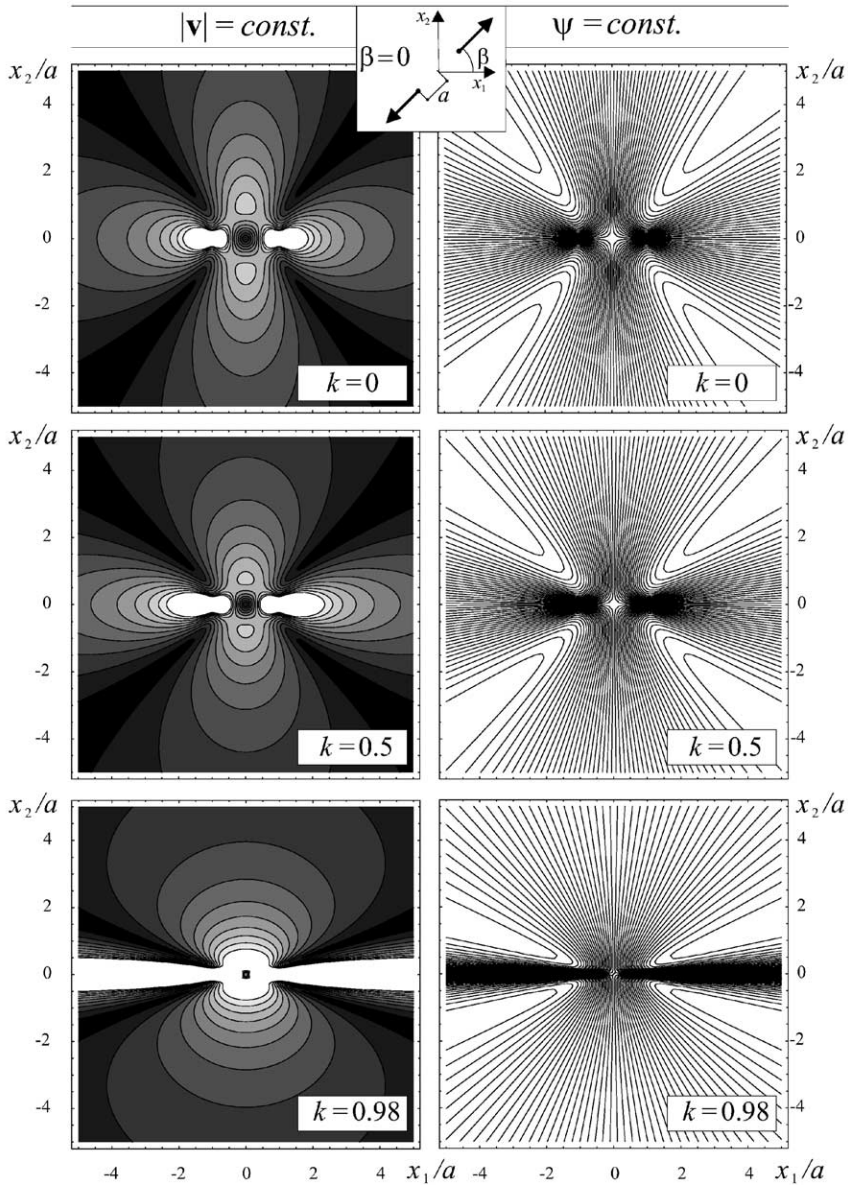

Fig. 3. Level sets of the modulus of velocity and streamlines for Mooney–Rivlin material, for a dipole aligned with axis x_1. The (EI)/(P) boundary is approached as the pre-stress k increases.

Figs. 6 and 7, relative to $\mu_*/\mu = 1/4$, correspond to a dipole aligned with axis x_1 ($\beta = 0$) and to different inclinations, respectively. In Fig. 6 a system of four shear bands develops at increasing k. These bands are inclined, with respect to axis x_1, at an angle corresponding to the inclination ($\approx 27.367^\circ$) calculated at the elliptic boundary

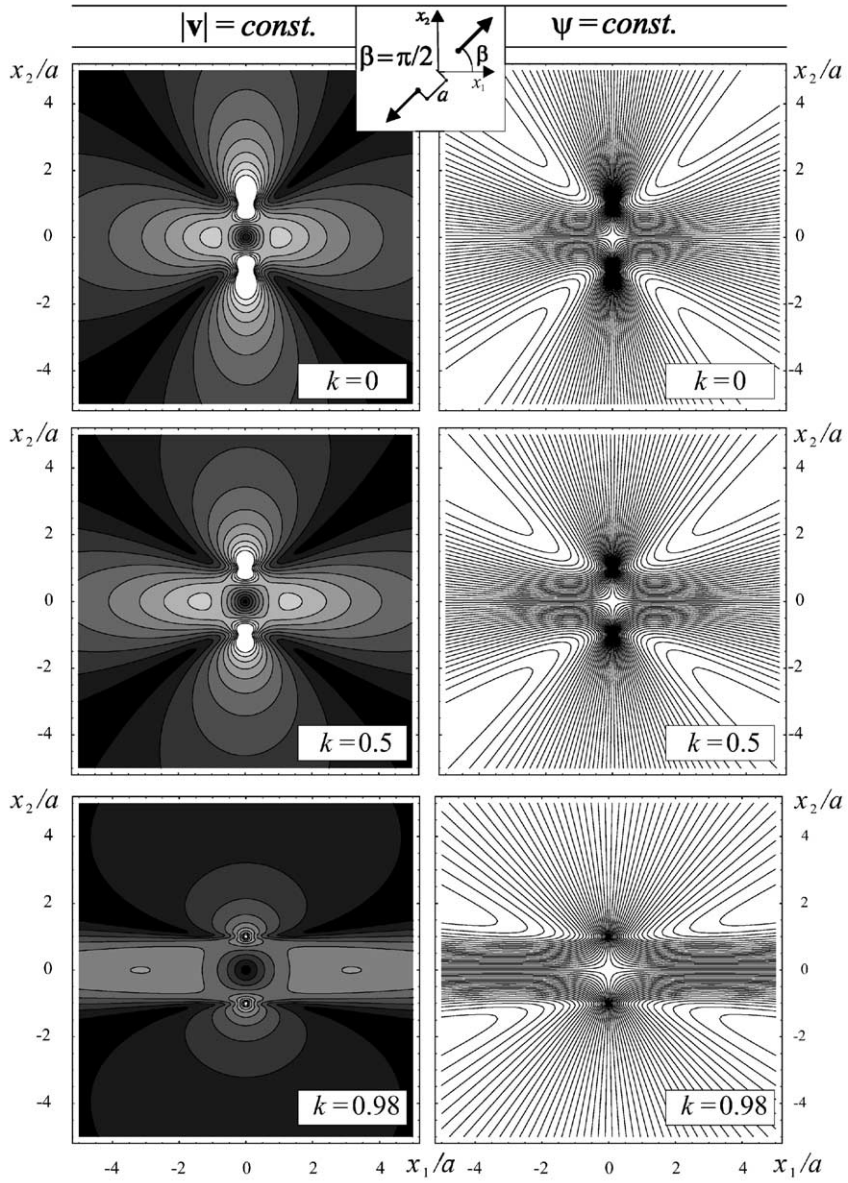

Fig. 4. Level sets of the modulus of velocity and streamlines for Mooney–Rivlin material, for a dipole aligned with axis x_2. The (EI)/(P) boundary is approached as the pre-stress k increases.

by the discontinuous shear band analysis. The level sets of the modulus of velocity are reported in Fig. 7 for $k = 0.86$ (corresponding to a point close to the (EC)/(H) boundary) and different inclinations β of the two-force system. The two inclinations $\beta = 27.367^\circ$ and 62.633° refer to the dipole directed along and orthogonal to the shear

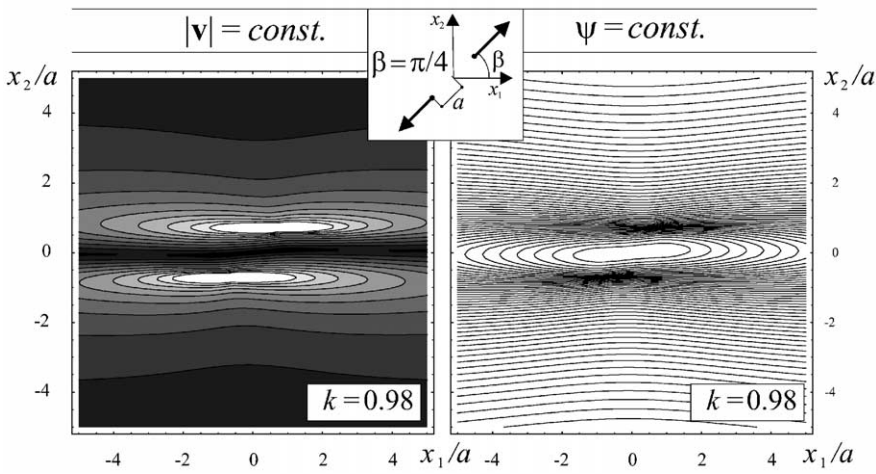

Fig. 5. Level sets of the modulus of velocity and streamlines for Mooney–Rivlin material, for $k = 0.98$ and a dipole inclined at 45°.

band calculated at the elliptic boundary. In the former case, $\beta = 27.367^\circ$, a mechanism consisting of three shear bands forms, one of which is thinner than the others. In the latter case, $\beta = 62.633^\circ$, only two shear bands form. For all other inclinations, four shear bands emerge.

Features similar to those evidenced in Figs. 3–7 were found for a broad range of material parameters and force inclinations (not reported here for conciseness). As a general conclusion, we may therefore point out that our results show that a perturbation during homogeneous deformation of a solid body (occurring close enough to the elliptic boundary) may induce localization of deformation still in the elliptic regime. Since localization occurs in the elliptic range, it might be concluded that regularization techniques are not needed to follow its subsequent growth. However, it is important to remark that the distance $2a$ between the two applied forces introduces a characteristic length in the problem, so that the band thickness will anyway depend on the geometry of perturbation.

5. Integral representations for velocity and hydrostatic stress rate in the incremental boundary value problem

Let us consider now a generic hyperelastic solid subjected to certain boundary conditions preserving homogeneous strain until the current state, assumed as the reference configuration. Superimposed infinitesimal deformation (generally inhomogeneous) is produced by incremental mixed boundary conditions in the usual form

$$v = \bar{v} \quad \text{on } \partial B_v \quad \text{and} \quad \dot{t}_{ij} n_i = \dot{\tau}_j \quad \text{on } \partial B_\tau, \tag{51}$$

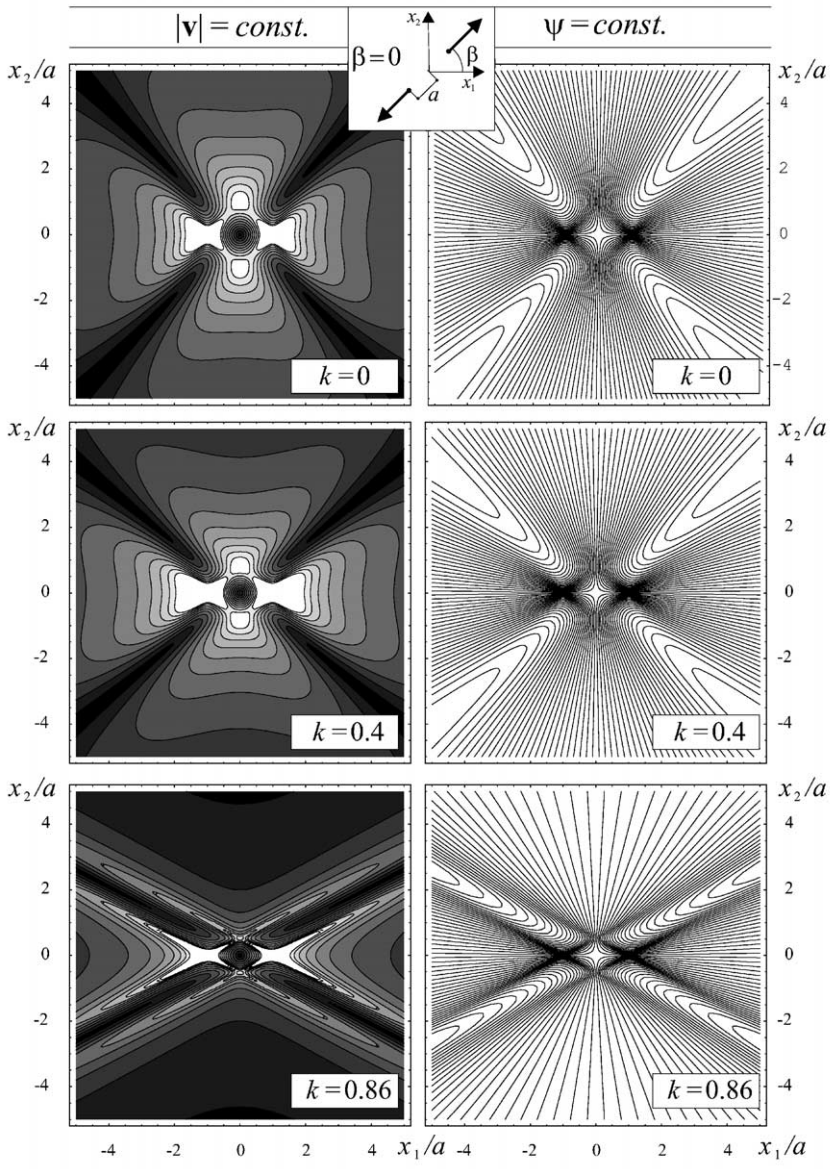

Fig. 6. Level sets of the modulus of velocity and streamlines for $\mu_*/\mu = 1/4$, for a dipole aligned with axis x_1. The (EC)/(H) boundary is approached at increasing pre-stress k.

where ∂B_v and ∂B_τ are the two nonoverlapping portions of the boundary where velocities and nominal traction rates are respectively prescribed. If we assume for simplicity null incremental body forces, superimposed nominal stress rates satisfy equilibrium

$$\dot{t}_{ij,i} = 0. \tag{52}$$

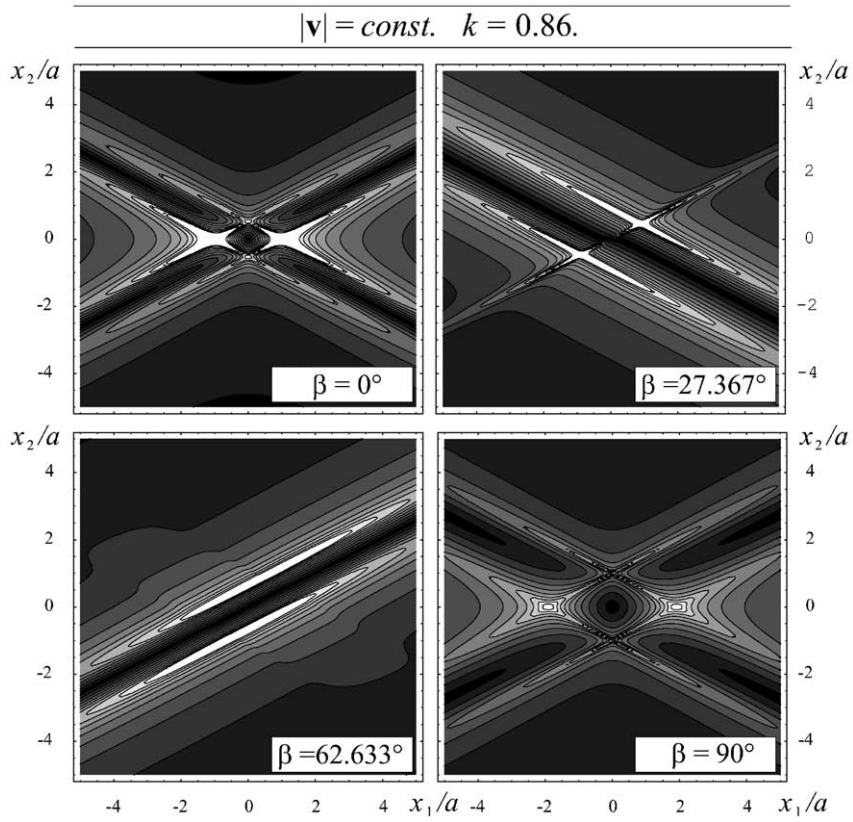

Fig. 7. Level sets of the modulus of velocity for $\mu_*/\mu = 1/4$ and $k = 0.86$, for a dipole at various inclinations with respect to axis x_1.

Moreover, the nominal stress rate $\dot{t}^g_{ij}(\boldsymbol{x},\boldsymbol{y})$ associated to the Green's function set $\{v^g_i, \dot{\pi}^g\}$ given by Eqs. (33) and (48) satisfies

$$\dot{t}^g_{ij,i} + \delta_{gj}\delta(\boldsymbol{x}-\boldsymbol{y}) = 0, \tag{53}$$

where $\boldsymbol{x}$ is the generic material point and $\boldsymbol{y}$ denotes the place where the force is applied, so that $r = |\boldsymbol{x}-\boldsymbol{y}|$ and $\vartheta = \tan^{-1}[(x_2-y_2)/(x_1-y_1)]$. Let us consider a disk C_ε of radius ε centered at $\boldsymbol{y}$. By integrating on the domain B–C_ε the scalar product of Eq. (53) with v_j and of Eq. (52) with v^g_j, we may write

$$\int_{B-C_\varepsilon} [\dot{t}^g_{ij,i}(\boldsymbol{x},\boldsymbol{y})v_j(\boldsymbol{x}) - \dot{t}_{ij,i}(\boldsymbol{x})v^g_j(\boldsymbol{x},\boldsymbol{y})]\,\mathrm{d}\boldsymbol{x} = 0. \tag{54}$$

An application of the divergence theorem yields

$$-\int_{\partial C_\varepsilon} [\dot{t}^g_{ij}(\boldsymbol{x},\boldsymbol{y})n_i v_j - \dot{t}_{ij}n_i v^g_j(\boldsymbol{x},\boldsymbol{y})]\,\mathrm{d}l_x = \int_{\partial B} [\dot{t}^g_{ij}(\boldsymbol{x},\boldsymbol{y})n_i v_j - \dot{t}_{ij}n_i v^g_j(\boldsymbol{x},\boldsymbol{y})]\,\mathrm{d}l_x, \tag{55}$$

where the major symmetry $\mathbb{K}_{ijkl} = \mathbb{K}_{klij}$ has been taken into account and n_i is the outward unit normal to ∂B and ∂C_ε.

Recalling now that $v_i^g \sim \log r$, it follows that

$$\lim_{\varepsilon \to 0} \int_{\partial C_\varepsilon} [\dot{t}_{ij} n_i v_j^g(\boldsymbol{x}, \boldsymbol{y})] \, \mathrm{d}l_x = 0, \tag{56}$$

and, consequently, Eq. (55) reduces in the limit $\varepsilon \to 0$ to

$$v_j(\boldsymbol{y}) C_j^g = \int_{\partial B} [\dot{t}_{ij} n_i v_j^g(\boldsymbol{x}, \boldsymbol{y}) - \dot{t}_{ij}^g(\boldsymbol{x}, \boldsymbol{y}) n_i v_j] \, \mathrm{d}l_x, \tag{57}$$

where

$$C_j^g = \lim_{\varepsilon \to 0} \int_{\partial C_\varepsilon} \dot{t}_{ij}^g(\boldsymbol{x}, \boldsymbol{y}) n_i \, \mathrm{d}l_x \tag{58}$$

is the so-called $\boldsymbol{C}$-matrix, which involves a regular integral, since $\dot{t}_{ij}^g \sim 1/r$. For interior points of B, an integration of Eq. (53) over C_ε and use of the properties of the delta function gives $C_j^g = \delta_{gj}$, so that

$$v_g(\boldsymbol{y}) = \int_{\partial B} [\dot{t}_{ij} n_i v_j^g(\boldsymbol{x}, \boldsymbol{y}) - \dot{t}_{ij}^g(\boldsymbol{x}, \boldsymbol{y}) n_i v_j] \, \mathrm{d}l_x. \tag{59}$$

Eq. (59) represents an integral equation relating the velocity in interior points of the body to the boundary values of nominal traction rates and velocities. Eq. (59) is formally similar to the analogous boundary integral equation in the infinitesimal theory.

In addition to Eq. (59), a boundary integral equation for the in-plane hydrostatic stress rate $\dot{p}$ is needed, to complete the boundary integral representation of field quantities. To this purpose, substituting the constitutive equation (1) into Eq. (52) we may express the gradient of $\dot{p}$ as a function of the second gradient of velocity. This may be obtained differentiating (59) twice with respect to $\boldsymbol{y}$, thus giving

$$\dot{p}_{,h}(\boldsymbol{y}) = - \int_{\partial B} \mathbb{K}_{nhsg} [\dot{t}_{ij} n_i v_{j,sn}^g(\boldsymbol{x}, \boldsymbol{y}) - \dot{t}_{ij,sn}^g(\boldsymbol{x}, \boldsymbol{y}) n_i v_j] \, \mathrm{d}l_x, \tag{60}$$

an expression in which the second derivatives in the integrand can be either performed with respect to $\boldsymbol{x}$ or $\boldsymbol{y}$, indifferently. For interior points, $\boldsymbol{x} \neq \boldsymbol{y}$, rate equilibrium requires that

$$\mathbb{K}_{nhsg} v_{j,sn}^g = \mathbb{K}_{nhsg} v_{g,sn}^j = - \dot{p}_{,h}^j, \tag{61}$$

where

$$\dot{p}^g = \dot{\pi}^g + \frac{\sigma}{2} v_{1,1}^g. \tag{62}$$

Taking Eqs. (61) and (62) into account, Eq. (60) becomes

$$\dot{p}_{,h}(\boldsymbol{y}) = \int_{\partial B} \dot{t}_{ig} n_i \dot{p}_{,h}^g(\boldsymbol{x}, \boldsymbol{y}) \, \mathrm{d}l_x + \int_{\partial B} \mathbb{K}_{nhsg} \dot{t}_{ij,sn}^g(\boldsymbol{x}, \boldsymbol{y}) n_i v_j \, \mathrm{d}l_x, \tag{63}$$

where $\dot{p}_{,h}^g$ is differentiated with respect to x_h. Using the constitutive relation (1) for $\dot{t}_{ij,sn}^g$ and the derivative of Eq. (61)

$$\mathbb{K}_{nhsg} v_{g,snk}^l = - \dot{p}_{,hk}^l \tag{64}$$

into Eq. (63), we get

$$\dot{p}_{,h}(\boldsymbol{y}) = \int_{\partial B} \dot{t}_{ig} n_i \dot{p}^g_{,h}(\boldsymbol{x},\boldsymbol{y})\,\mathrm{d}l_x - \int_{\partial B} n_i v_j \mathbb{K}_{ijkg} \dot{p}^g_{,hk}(\boldsymbol{x},\boldsymbol{y})\,\mathrm{d}l_x + \int_{\partial B} n_i v_i \mathbb{K}_{nhsg} \dot{p}^g_{,sn}(\boldsymbol{x},\boldsymbol{y})\,\mathrm{d}l_x. \tag{65}$$

It should be noted that—with a change in sign—a derivative with respect to y_h can be extracted from the first two integrals on the right-hand side of Eq. (65). Moreover, it is proved in Appendix B that

$$\mathbb{K}_{nhsg} \dot{p}^g_{,sn} = \left[\left(4\mu\mu_* - 4\mu_*^2 + \mu\sigma - 2\mu_*\sigma - \frac{\sigma^2}{2} \right) v^1_{1,11} - \sigma \left(\mu + \frac{\sigma}{2} \right) v^2_{2,11} \right]_{,h}, \tag{66}$$

so that Eq. (65) can be integrated with respect to y_h, yielding

$$\dot{p}(\boldsymbol{y}) = -\int_{\partial B} \dot{t}_{ig} n_i \dot{p}^g(\boldsymbol{x},\boldsymbol{y})\,\mathrm{d}l_x + \int_{\partial B} n_i v_j \mathbb{K}_{ijkg} \dot{p}^g_{,k}(\boldsymbol{x},\boldsymbol{y})\,\mathrm{d}l_x - \int_{\partial B} n_i v_i \left[\left(4\mu\mu_* - 4\mu_*^2 + \mu\sigma - 2\mu_*\sigma - \frac{\sigma^2}{2} \right) v^1_{1,11}(\boldsymbol{x},\boldsymbol{y}) - \sigma \left(\mu + \frac{\sigma}{2} \right) v^2_{2,11}(\boldsymbol{x},\boldsymbol{y}) \right] \mathrm{d}l_x, \tag{67}$$

where $\dot{p}^g_{,k}$ is differentiated with respect to x_k. Moreover, it is worth noting that the signs opposite to Eq. (65) are a consequence of integration with respect to $\boldsymbol{y}$ and that the constant of integration is null. The latter fact can be explained noting that Eq. (67) holds for every closed contour ∂B internal to the body and also for points $\boldsymbol{y}$ external to the body, where $\dot{p} = 0$. Therefore, considering external points, the integrands in Eq. (67) are bounded, so that the integrals tend to zero when the contour of integration shrinks to a point and this implies vanishing of the integration constant.

Eq. (67) represents an integral equation relating the in-plane hydrostatic stress rate in the interior points of the body to the boundary values of nominal traction rates and velocities. For null pre-stress ($\sigma = 0$) and isotropy ($\mu = \mu_*$), the boundary integral equation (67) becomes formally analogous to the corresponding equation for incompressible, viscous flow (Ladyzhenskaya, 1963, Section 3.2).

6. Boundary element technique

The boundary integral equation (57) may be used as the starting point for developing a boundary element technique to solve problems of incremental deformations superimposed upon a given homogeneous strain. To this purpose, we note that Eq. (59) gives the velocity field in the interior points of the body. In order to obtain the velocity field *on the boundary* of the body, we take the source point $\boldsymbol{y}$ to the boundary and re-write Eq. (57), where the integral becomes a Cauchy principal value integral; consequently, the $\boldsymbol{C}$-matrix (58) is re-defined as

$$C^g_j(\boldsymbol{y}) = \lim_{\varepsilon \to 0} \int_{\Gamma_\varepsilon} \dot{t}^g_{ij}(\boldsymbol{x},\boldsymbol{y}) n_i\,\mathrm{d}l_x, \tag{68}$$

Table 1
C-matrix for Mooney–Rivlin material

k	$p/\mu=-k$		$p/\mu=k$	
	C_2^1	C_1^2	C_2^1	C_1^2
0	0.15915	0.15915	0.15915	0.15915
0.2	0.19759	0.15807	0.15807	0.13172
0.4	0.25749	0.15449	0.15449	0.11035
0.6	0.36773	0.14709	0.14709	0.09193
0.8	0.65569	0.13114	0.13114	0.07285

where Γ_ε is the intersection of the circle of radius ε centered at $\boldsymbol{y}$ with the region occupied by the body and, consistently with Eq. (58), the outward unit normal n_i points towards $\boldsymbol{y}$. Using polar coordinates r and ϑ with origin at $\boldsymbol{y}$, definition (68) becomes

$$C_j^g = \int_{\vartheta_0}^{\vartheta_1} \dot{t}_{ij}^g(r,\vartheta) n_i(\vartheta) r \, \mathrm{d}\vartheta, \tag{69}$$

where ϑ_0 and ϑ_1 are the angular coordinates of the half-tangents to the boundary at point $\boldsymbol{y}$. As expected, since $\dot{t}_{ij}^g \sim 1/r$, the integrand in Eq. (69) is independent of r.

At a smooth point of the boundary, elementary considerations of symmetry are sufficient to conclude that

$$C_j^g = \frac{1}{2}\delta_{gj}, \tag{70}$$

whereas, for piecewise smooth boundary, the $\boldsymbol{C}$-matrix turns out to be generally unsymmetrical at a corner. In this case, the terms of the $\boldsymbol{C}$-matrix depend on the nondimensionalized pre-stress k, the hydrostatic stress p/μ and on the ratio μ_*/μ. For instance, let us take $\boldsymbol{y}$ at the corner of a right angle. Due to symmetry considerations, $C_1^1 = C_2^2 = 1/4$ for any value of material parameters and pre-stress, but the out-of-diagonal terms depend on k, p/μ and μ_*/μ. In particular, some out-of diagonal terms are reported in Table 1 for Mooney–Rivlin material and different values of nondimensional pre-stress k and hydrostatic stress p/μ. Note that the $\boldsymbol{C}$-matrix becomes symmetrical in the special case of a null pre-stress.

In order to implement a boundary element technique, the contour of the body has to be discretized into finite elements and appropriate shape functions for velocity and nominal traction rate have to be chosen. By collocating the integral equation (57) with the $\boldsymbol{C}$-matrix (69) at the element nodes, a linear algebraic system is obtained, for the unknown nodal values of velocities and nominal traction rates. Obviously, the determination of the coefficients of the algebraic system requires the evaluation of weakly singular integrals (involving the Green's functions v_i^g) and of Cauchy principal value integrals (related to the nominal stress rate $\dot{t}_{ij}^g$ of the Green's state). Once the boundary quantities are known, the interior fields may be readily obtained using Eq. (59) for the velocity and Eq. (67) for the in-plane hydrostatic stress rate.

An application of the boundary element technique to the solution of an incremental boundary value problem is developed below.

6.1. Example: a perturbative approach to bifurcation of an elastic block

In the current configuration, a square elastic block in plane strain conditions is considered, subject to uniaxial, compressive stress. For simplicity, the analysis is restricted to Mooney–Rivlin material, for which the axial stress and incremental moduli are provided by Eq. (5). Planar, smooth, rigid constraints maintain the uniform compression (Biot, 1965; Hill and Hutchinson, 1975; Young, 1976) and, starting from this configuration, a symmetric perturbation is assigned as an incremental nominal traction, acting orthogonally to a portion of the free edges of the block (see the particular of Fig. 8). In order to determine the nominal traction rates on the constrained ends and the velocities on the free edges of the block, the boundary element procedure is applied. The boundary is discretized using linear shape functions for velocities and nominal stress rates.

Uniform meshes have been chosen, so that having elements of equal length avoids the problem of evaluating strongly singular contributions to the integrals in Eq. (57). These can be shown to be zero on the basis of the following identities:

$$\dot{t}^1_{11}(r,\vartheta=\pi/2)=\dot{t}^1_{11}(r,\vartheta=-\pi/2)=0,\quad \dot{t}^1_{21}(r,\vartheta=0)=\dot{t}^1_{21}(r,\vartheta=\pi)=0, \tag{71}$$

when the collocation node is located at a free edge, and

$$\dot{t}^2_{11}(r,\vartheta=-\pi/2)=-\dot{t}^2_{21}(r,\vartheta=\pi),\quad \dot{t}^1_{12}(r,\vartheta=-\pi/2)=-\dot{t}^1_{22}(r,\vartheta=\pi), \tag{72}$$

when the collocation node is located at a corner. Identities (71) follow from symmetry considerations, whereas identities (72) are derived in Appendix C.

The loaded portion has been taken equal to $1/9$ of the edge length. Two meshes having 72 and 144 elements of equal length have been employed. The results of numerical investigation are reported in Figs. 8 and 9. The velocity v_C at the middle point of the edge (nondimensionalized as $\mu v_C/(b\dot{\tau})$, where b is the half-length of the edge and $\dot{\tau}$ is the applied nominal traction rate) is plotted versus the pre-stress k. The computed values are marked by a spot. The values $k=\{0,0.2,0.4,0.6,0.7,0.8,0.82,0.84,0.845\}$ have been reported in Fig. 8 for the fine mesh and $k=\{0,0.2,0.4,0.6,0.7,0.8,0.82,0.84,0.86,0.868\}$ for the coarse mesh. The profiles of velocity components [multiplied by $\mu/(b\dot{\tau})$] along the edge are shown in Fig. 9, for different values of k. In both figures, comparisons are also included with results obtained using ABAQUS-Standard (Ver. 5.8-Hibbitt, Karlsson and Sorensen Inc, Pawtucket, RI), with plane-strain, 4-node, bilinear, hybrid elements (CPE4H). In particular, the following procedure within the ABAQUS environment has been adopted. Starting from an unloaded configuration of a rectangular block, this is biaxially deformed until a square configuration subject to a desired value of axial compression k is reached. The initial mesh is chosen so that at this stage of deformation the elements are square and have the same number of nodes on the edges of the fine boundary element discretization. At this point, the incremental loading is given in the prescribed zones of the edges and the linear incremental problem is solved (option PERTURBATION).

A progressive degradation of stiffness in the response may be noted from Fig. 8, when the level of pre-stress is increased. The curves relative to two meshes exhibit

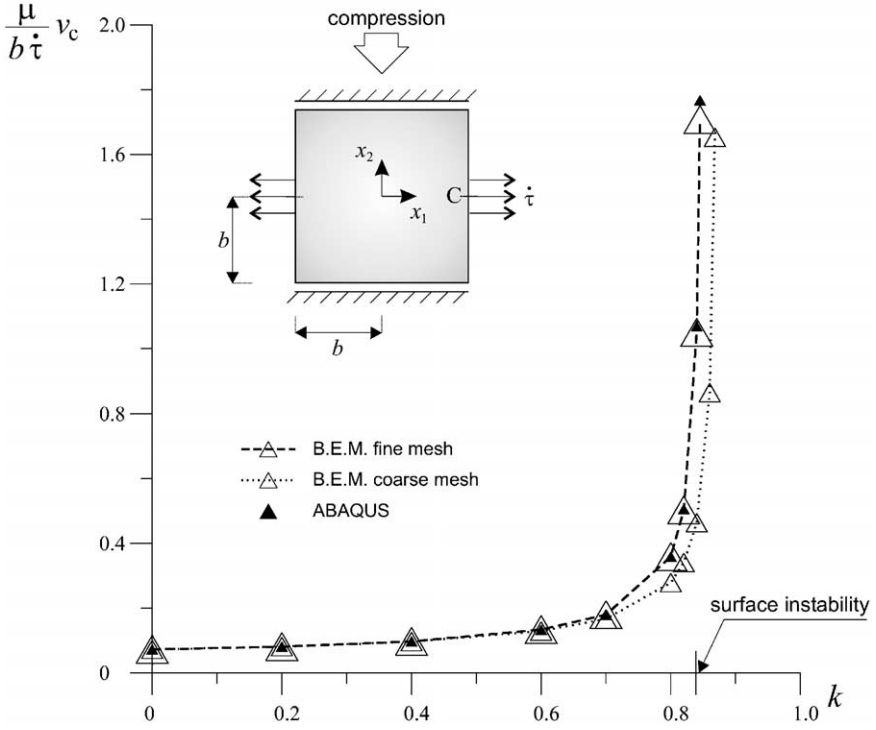

Fig. 8. Velocity of the central point C (multiplied by $\mu/b\dot{\tau}$) versus pre-stress k.

asymptotes at critical values of k between 0.849 and 0.850 for the fine mesh, and between 0.880 and 0.881 for the coarse mesh.

Profiles of components of velocities along the edge are shown in Fig. 9 for $k = \{0, 0.4, 0.845\}$. Results relative to the fine mesh are represented by a continuous curve along the edge, whereas results obtained by ABAQUS are marked with spots in the upper part of the edge (positive values of x_2/b) and results obtained with the coarse mesh are reported in the lower part of the edge (negative values of x_2/b). Results of ABAQUS are always in excellent agreement with our results, except for the component v_2 in the case $k = 0$. In this particular case, comparisons with results of ABAQUS obtained using fine meshes (not reported here) show that our results are the most accurate. Results relative to the coarse and the fine meshes are in good agreement, except for high values of pre-stress. This can be explained as follows. For increasing values of k, the corresponding profiles of velocity undergo a shape variation and evolve towards the profile associated to a bifurcation mode. This can clearly be observed in Fig. 9. To understand this point in detail, we have to recall results from bifurcation analysis of a rectangular elastic block (Biot, 1965; Hill and Hutchinson, 1975; Young, 1976). For Mooney–Rivilin material, bifurcations in anti-symmetric modes always occur at values of pre-stress lower than those relative to symmetric bifurcations. For a square geometry, the first anti-symmetric bifurcation occurs at $k \approx 0.522$. Since the incremental

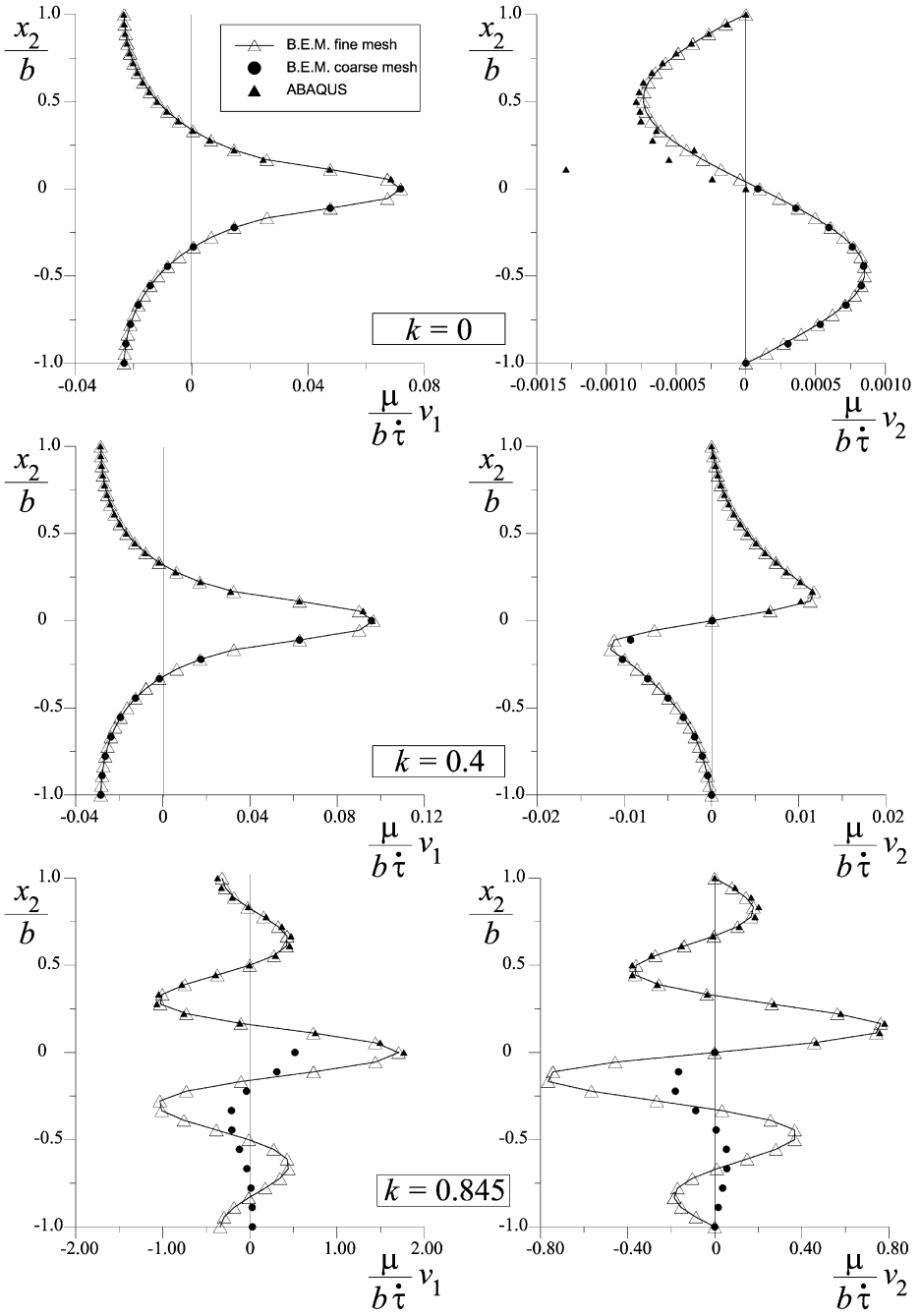

Fig. 9. Velocity profiles (multiplied by $\mu/b\dot{\tau}$) along the free edge.

Table 2
Some critical values of pre-stress and wavelength of the associated symmetric bifurcation mode for Mooney–Rivlin material

k	$\lambda/2b$
0.926	1.5
0.866	2
0.849	2.5
0.843	3
0.841	3.5
0.840	4
⋮	⋮
0.839	∞

load $\dot{\tau}$ is symmetrical, such a bifurcation mode and, in general, anti-symmetric modes are not activated in the present example (Fig. 8). On the other hand, the first symmetric bifurcation occurs at the surface instability limit $k \approx 0.839$. This limit value is an accumulation point for pre-stress associated to both symmetric and anti-symmetric bifurcation modes. In particular, the highest value of k for a symmetric bifurcation is $k \approx 0.925$, corresponding to a mode with wavelength $\lambda/2b = 1.5$. All infinite values of k for symmetric bifurcation range between the two above extreme values. Some of these values are reported in Table 2, obtained using Eq. (6.2) of Young (1976). The two deformation profiles relative to the asymptotes in Fig. 8 correspond to bifurcation modes $\lambda/2b = 3$ for the fine mesh, and $\lambda/2b = 2$ for the coarse mesh. The values of k corresponding to the asymptotes in Fig. 8 are higher than those predicted from the bifurcation analysis (Table 2). This is consistent with the fact that the discretization makes the system stiffer, so that the finer is the mesh, the more the surface instability threshold is approached.

7. Conclusions

A Green's function for an infinite body and a boundary integral formulation for velocity and hydrostatic stress rate have been obtained in the framework of incremental elastic deformations superimposed upon a given homogeneous strain. The above results have been exploited in two different directions. First, decay of self-equilibrated loads and related material instabilities have been investigated. A perturbative approach to shear bands occurring within the elliptic range has been proposed. We believe that similar perturbative techniques could be used in different contexts, to investigate other instabilities, as for instance flutter in a dynamic context. Second, the boundary integral equations have been employed to build up a boundary element technique for incremental elastic deformation. This technique may become particularly convenient in view of the incompressibility constraint typical of elastic deformations. Although limited to incremental deformations superimposed upon a given homogeneous strain, the proposed boundary element technique paves the way for a rigorous approach to finite elasticity via boundary elements.

Acknowledgements

D.B. gratefully acknowledges financial support from University of Trento (Trento, Italy), D.C. thanks financial support from M.U.R.S.T. (University of Ferrara, Ferrara, Italy).

Appendix A. Behaviour of Green's tensor components at the elliptic boundary

According to Eq. (32), component v_2^1 is given by

$$v_2^1 = \frac{1}{2\pi^2\mu(1+k)} \int_0^\pi \frac{\cos(\alpha+\vartheta)\sin(\alpha+\vartheta)}{\Lambda(\alpha+\vartheta)} \log|\cos\alpha|\,\mathrm{d}\alpha, \tag{A.1}$$

which may be re-written as

$$v_2^1 = \frac{1}{2\pi^2\mu(1+k)} \int_0^\pi \frac{\cos\alpha\sin\alpha}{\Lambda(\alpha)} \log|\cos(\alpha-\vartheta)|\,\mathrm{d}\alpha. \tag{A.2}$$

At the elliptic boundary, where shear bands become possible, $\Lambda(\alpha)$ vanishes for values of α characterizing normals to shear bands. In particular, at the (EI)/(P) boundary, $\Lambda(\alpha)$ vanishes when $\alpha = \pi/2$, whereas at the (EC)/(H) boundary $\Lambda(\alpha)$ vanishes when $\alpha = \alpha_n$ and $\alpha = \pi - \alpha_n$, with α_n ranging between $\pi/4$ and $\pi/2$ and denoting the angle between the normal to a shear band and the axis x_1.

When approaching the (EC)/(H) boundary, a small positive β can be considered such that integral (A.2) may be sub-divided into

$$\int_0^\pi [\ ] = \int_0^{\alpha_n-\beta} [\ ] + \int_{\alpha_n-\beta}^{\alpha_n+\beta} [\ ] + \int_{\alpha_n+\beta}^{\pi-\alpha_n-\beta} [\ ] + \int_{\pi-\alpha_n-\beta}^{\pi-\alpha_n+\beta} [\ ] + \int_{\pi-\alpha_n+\beta}^{\pi} [\ ], \tag{A.3}$$

so that the singularity of Eq. (A.2) can be condensed in the contribution

$$\frac{1}{2\pi^2\mu(1+k)} \int_{\alpha_n-\beta}^{\alpha_n+\beta} \frac{\cos\alpha\sin\alpha}{\Lambda(\alpha)} \log\left|\frac{\cos(\alpha-\vartheta)}{\cos(\alpha+\vartheta)}\right| \mathrm{d}\alpha. \tag{A.4}$$

With the exception of $\vartheta = n\pi/2$ ($n = 0, 1, 2, \ldots$) where $v_2^1 = 0$, integral (A.4) diverges and consequently v_2^1 goes to infinity when approaching the (EC)/(H) threshold. A similar argument can be applied to show that components v_1^1 and v_2^2 diverge in the (EC)/(H) limit.

When approaching the (EI)/(P) boundary, i.e. taking the limit $\gamma_1 \to 0^-$, a small positive β can be considered such that the singularity is condensed in the contribution

$$\frac{1}{2\pi^2\mu(1+k)} \lim_{\gamma_1\to 0^-} \int_{\pi/2-\beta}^{\pi/2+\beta} \frac{\cos\alpha\sin\alpha}{\Lambda(\alpha)} \log|\cos(\alpha-\vartheta)|\,\mathrm{d}\alpha. \tag{A.5}$$

Now, being $\cos\alpha\sin\alpha/\Lambda(\alpha)$ an odd function of α, we note that

$$\int_{\pi/2-\beta}^{\pi/2+\beta}\frac{\cos\alpha\sin\alpha}{\Lambda(\alpha)}\log|\cos(\alpha-\vartheta)|\,\mathrm{d}\alpha$$

$$=\int_{\pi/2-\beta}^{\pi/2+\beta}\frac{\cos\alpha\sin\alpha}{\Lambda(\alpha)}[\log|\cos(\alpha-\vartheta)|-\log|\cos(\pi/2-\vartheta)|]\,\mathrm{d}\alpha \tag{A.6}$$

where the integrand on the right-hand side is not singular when $\gamma_1=0$. Hence, Eq. (A.5) remains finite at the (EI)/(P) boundary and, in particular, the component v_2^1 tends to

$$v_2^1=\frac{1}{2\pi^2\mu(1+k)}\,\text{P.V.}\int_0^{\pi}\frac{\tan\alpha}{\cos^2\alpha-\gamma_2\sin^2\alpha}\log|\cos(\alpha-\vartheta)|\,\mathrm{d}\alpha. \tag{A.7}$$

Finally, when approaching the (EI)/(P) boundary, the singularity in v_1^1 is represented by

$$\frac{-1}{2\pi^2\mu(1+k)}\lim_{\gamma_1\to0^-}\int_{\pi/2-\beta}^{\pi/2+\beta}\frac{\sin^2\alpha}{\Lambda(\alpha)}\log|\hat{r}\cos(\alpha-\vartheta)|\,\mathrm{d}\alpha, \tag{A.8}$$

which can easily be shown to diverge.

Appendix B. Derivation of relation (66)

The components of $\mathbb{K}_{nhsg}\dot{p}^g_{,sn}$ are

$$\mathbb{K}_{n1sg}\dot{p}^g_{,sn}=\left(\mu_*-\frac{\sigma}{2}-p\right)\dot{p}^1_{,11}+(\mu-\mu_*-p)\dot{p}^2_{,12}+\left(\mu-\frac{\sigma}{2}\right)\dot{p}^1_{,22},$$

$$\mathbb{K}_{n2sg}\dot{p}^g_{,sn}=\left(\mu_*+\frac{\sigma}{2}-p\right)\dot{p}^2_{,22}+(\mu-\mu_*-p)\dot{p}^1_{,12}+\left(\mu+\frac{\sigma}{2}\right)\dot{p}^2_{,11}. \tag{B.1}$$

Using Eq. (64), which rewritten with the above indices reads

$$\dot{p}^g_{,sn}=-\mathbb{K}_{pnqr}v^g_{r,qps}, \tag{B.2}$$

we calculate the components of $\dot{p}^g_{,sn}$

$$\dot{p}^g_{,11}=-\left(2\mu_*-\mu-\frac{\sigma}{2}\right)v^g_{1,111}-\left(\mu-\frac{\sigma}{2}\right)v^g_{1,122},$$

$$\dot{p}^g_{,22}=\left(2\mu_*-\mu+\frac{\sigma}{2}\right)v^g_{1,122}-\left(\mu+\frac{\sigma}{2}\right)v^g_{2,112},$$

$$\dot{p}^g_{,21}=\left(2\mu_*-\mu+\frac{\sigma}{2}\right)v^g_{1,121}-\left(\mu+\frac{\sigma}{2}\right)v^g_{2,111},$$

$$\dot{p}^g_{,12}=-\left(2\mu_*-\mu-\frac{\sigma}{2}\right)v^g_{1,121}-\left(\mu-\frac{\sigma}{2}\right)v^g_{1,222}, \tag{B.3}$$

where

$$\dot{p}^g_{,12}=\dot{p}^g_{,21}. \tag{B.4}$$

A substitution of Eq. (B.3) into Eq. $(B.1)_1$ gives

$$\mathbb{K}_{n1sg}\dot{p}^{g}_{,sn}=\left(4\mu\mu_{*}-4\mu_{*}^{2}-\mu\sigma+2\mu_{*}\sigma-\frac{\sigma^{2}}{2}\right)v^{1}_{1,111}-\sigma\left(\mu-\frac{\sigma}{2}\right)v^{1}_{2,222}, \tag{B.5}$$

which, using Eq. (B.4), may be transformed into

$$\mathbb{K}_{n1sg}\dot{p}^{g}_{,sn}=\left[\left(4\mu\mu_{*}-4\mu_{*}^{2}+\mu\sigma-2\mu_{*}\sigma-\frac{\sigma^{2}}{2}\right)v^{1}_{1,11}-\sigma\left(\mu+\frac{\sigma}{2}\right)v^{2}_{2,11}\right]_{,1}. \tag{B.6}$$

A substitution of Eq. (B.3) into $(B.1)_2$ gives

$$\mathbb{K}_{n2sg}\dot{p}^{g}_{,sn}=\left[\left(4\mu\mu_{*}-4\mu_{*}^{2}+\mu\sigma-2\mu_{*}\sigma-\frac{\sigma^{2}}{2}\right)v^{1}_{1,11}-\sigma\left(\mu+\frac{\sigma}{2}\right)v^{2}_{2,11}\right]_{,2}, \tag{B.7}$$

which, together with Eq. (B.6), gives the components of Eq. (66).

Appendix C. Derivation of identities (72)

Using constitutive equations, identities (72) are equivalent to

$$2\mu_{*}v^{2}_{1,1}(-\pi/2)+\dot{\pi}^{2}(-\pi/2)=-\mu v^{2}_{2,1}(\pi)-\left(\mu-\frac{\sigma}{2}\right)v^{2}_{1,2}(\pi), \tag{C.1}$$

$$\left(\mu+\frac{\sigma}{2}\right)v^{1}_{2,1}(-\pi/2)+(\mu-p)v^{1}_{1,2}(-\pi/2)=-(2\mu_{*}-p)v^{1}_{2,2}(\pi)-\dot{\pi}^{1}(\pi). \tag{C.2}$$

Using Eqs. (32) together with Eqs. (36) and (41), we obtain

$$v^{2}_{1,1}(-\pi/2)=-v^{2}_{2,2}(-\pi/2)=-v^{2}_{2,1}(\pi)=-\frac{1}{2\pi^{2}\mu(1+k)r}\int_{0}^{\pi}\frac{\cos^{2}\alpha}{\Lambda(\alpha)}\,\mathrm{d}\alpha, \tag{C.3}$$

$$v^{2}_{1,2}(\pi)=-v^{1}_{1,1}(\pi)=-v^{1}_{1,2}(-\pi/2)=-\frac{1}{2\pi^{2}\mu(1+k)r}\int_{0}^{\pi}\frac{\sin^{2}\alpha}{\Lambda(\alpha)}\,\mathrm{d}\alpha, \tag{C.4}$$

$$\dot{\pi}^{1}(\pi)=\frac{1}{2\pi^{2}r}\int_{0}^{\pi}\left[1-\frac{\sin^{2}\alpha}{(1+k)\Lambda(\alpha+\pi)}\Gamma(\alpha+\pi)\right]\mathrm{d}\alpha, \tag{C.5}$$

$$\dot{\pi}^{2}(-\pi/2)=\frac{1}{2\pi^{2}r}\int_{0}^{\pi}\left[1+\frac{\sin^{2}\alpha}{(1+k)\Lambda(\alpha-\pi/2)}\Gamma(\alpha-\pi/2)\right]\mathrm{d}\alpha. \tag{C.6}$$

Substitution of Eqs. (C.3)–(C.6) into Eqs. (C.1) and (C.2) proves identities (72).

References

Abeyaratne, R., Horgan, C.O., Chung, D-T., 1985. Saint-Venant end effects for incremental plane deformations of incompressible nonlinearly elastic materials. J. Appl. Mech. 52, 847–852.

Beatty, M.F., Usmani, S.A., 1975. On the indentation of a highly elastic half-space. Quart. J. Mech. Appl. Math. XXVIII, 47–62.

Biot, M.A., 1965. Mechanics of Incremental Deformations. Wiley, New York.

Courant, R., Hilbert, D., 1962. Methods of Mathematical Physics, Vol. II. Wiley, New York.
Dhaliwal, R.S., Singh, B.M., 1978. The axisymmetric Boussinesq problem of an initially stretched neo-Hookean half-space for a punch of arbitrary profile. Int. J. Eng. Sci. 16, 379–385.
Durban, D., Stronge, W.J., 1988. Diffusion of self-equilibrating end loads in elastic solids. J. Appl. Mech. 55, 492–495.
Filippova, L.M., 1978. Three-dimensional contact problem for a prestressed elastic body. PMM 42, 1183–1187.
Gel'fand, I.M., Shilov, G.E., 1964. Generalized Functions, Vol. 1, Properties and Operations. Academic Press, New York.
Green, A.E., Rivlin, R.S., Shield, R.T., 1952. General theory of small elastic deformations superposed on large elastic deformations. Proc. Roy. Soc. A 211, 128–154.
Green, A.E., Zerna, W., 1968. Theoretical elasticity, 2nd Edition. Oxford University Press, London.
Gurtin, M.E., 1972. The linear theory of Elasticity. In: Flügge, S. (Ed.), Encyclopedia of Physics, Vol. VIa/2. Springer, Berlin, pp. 1–295.
Guz', A.N., Babich, S.Y., Rudnitsky, V.B., 1998. Contact problems for elastic bodies with initial stresses: focus on Ukranian research. Appl. Mech. Rev. 51, 343–371.
John, F., 1955. Plane Waves and Spherical Means. Springer, New York.
Hill, R., Hutchinson, J.W., 1975. Bifurcation phenomena in the plane tension test. J. Mech. Phys. Solids 23, 239–264.
Horgan, C.O., 1989. Recent developments concerning Saint-Venant's principle: an update. Appl. Mech. Rev. 42, 295–303.
Horgan, C.O., 1996. Recent developments concerning Saint-Venant's principle: a second update. Appl. Mech. Rev. 49, S101–S111.
Hutchinson, J.W., Neale, K.W., 1979. Finite strain J_2-deformation theory. In: Carlson, D.E., Shield, R.T. (Eds.), IUTAM Symposium on Finite Elasticity. Martinus Nijhoff, The Hague, pp. 237–247.
Ladyzhenskaya, O.A., 1963. The Mathematical Theory of Viscous Incompressible Flow. Gordon and Breach, New York.
Lifshitz, I.M., Rozentsveig, L.N., 1947. Construction of the Green tensor for the fundamental equation of elasticity theory in the case of an unbounded elastically anisotropic medium. Zh. Eksp. Teor. Fiz. 17, 783–791.
Love, A.E.H., 1927. A Treatise on the Mathematical Theory of Elasticity, 4th Edition. Cambridge University Press, Cambridge.
Mises, R. von, 1945. On Saint Venant's principle. Bull. Am. Math. Soc. 51, 555–562.
Ogden, R.W., 1984. Non-linear Elastic Deformations. Ellis Horwood, Chichester.
Pan, Y.-C., Chou, T.-W., 1976. Point force solution for an infinite transversely isotropic solid. J. Appl. Mech. 43, 608–612.
Ting, T.C.T., Lee, V.-G., 1997. The three-dimensional elastostatic Green's function for general anisotropic linear elastic solids. Quart. J. Mech. Appl. Math. 50, 407–426.
Willis, J.R., 1965. The elastic interaction energy of dislocation loops in anisotropic media. Quart. J. Mech. Appl. Math. XVIII, 419–433.
Willis, J.R., 1971. Interfacial stresses induced by arbitrary loading of dissimilar elastic half-spaces joined over a circular region. J. Inst. Math. Appl. 7, 179–197.
Willis, J.R., 1972. The penny-shaped crack on an interface. Quart. J. Mech. Appl. Math. XXV, 367–385.
Willis, J.R., 1973. Self-similar problems in elastodynamics. Philos. Trans. Roy. Soc. London A 274, 435–491.
Willis, J.R., 1991. Inclusions and cracks in constrained anisotropic media. In: Wu, J.J., Ting, T.C.T., Barnett, D.M. (Eds.), Modern Theory of Anisotropic Elasticity and Applications. SIAM, Philadelphia, pp. 87–102.
Young, N.J.B., 1976. Bifurcation phenomena in the plane compression test. J. Mech. Phys. Solids 24, 77–91.
Zanaboni, O., 1937. Dimostrazione generale del principio del de Saint Venant. Atti Accad. Lincei Rend. 25, 117–121.